A Study on Online Corrosion Risk Perception Technology for Process Industry Safety IoTs Based on Demands of Assets Integrity Management

Liang Xiong[1], Guanglei Lv[2], Guangpei Cong[3(✉)], Fengqi He[4], Shi He[5], and Yunjiang Sun[2]

[1] China University of Geosciences, Wuhan, China
[2] CNOOC Safety Environmental Protection Engineering Technology Research Institute, Beijing, China
[3] Guangdong University of Petrochemical Technology, Maoming, China
125414712@qq.com
[4] Nuclear Power Institute of China, Beijing, China
[5] Nuclear Industry Management Cadre Institute, Beijing, China

Abstract. Combining developing demand on process industry safety management, an safety risk perception system for the process industry safety IoTs was proposed to a corrosion loop in a process unit. A low-dose tangential wall thickness measurement sensor based on gamma ray was adopted by this system. In addition, basic principle for realizing boundary layer recognition of the sensor was presented together with a precision measurement algorithm. In addition to merits such as without destroying insulation constructions and high-precision wall thickness measurement, the sensor of this system could be installed or dismantled online with a low cost, etc. With the system, the safety condition of a corrosion loop can be directly real-time soft measured quantitatively which is the foundation to establish the process industry safety IoTs.

Keywords: Process industry · Automatic monitoring system
Gamma ray sensor

1 Introduction

According to statistics, billions of losses in dollar are caused by corrosions under the heat insulation layer in the petroleum chemical industry [7]. Furthermore, severe corrosions are also able to lead to equipment failures and non-plan shutdown in manufacturing plants and the leakage of dangerous and harmful factors may also give rise to life casualties [8]. In most cases, such pipelines under high risks are equipped with external tube structures such as a heat insulation layer. Therefore, in a production state, it is extremely difficult to directly employ inspection techniques to perform safety management.

Research of Bruce and Lv et al. [9, 10] indicate that the serious corrosion probability for devices or pipelines under the heat insulation layer currently applied goes up

Y.-B. Lin et al. (Eds.): IoTaaS 2017, LNICST 246, pp. 155–169, 2018.
https://doi.org/10.1007/978-3-030-00410-1_19

with the time. According to Geary, Kane and Norsworthy [11–13], as water is a critical factor incurring corrosion under insulation, corrosion phenomena become especially prominent in marine environment where the concentration of chloridion contained in corrosive media is even greater. Therefore, corrosion management for pipelines incorporating any heat insulation layer becomes particularly important. For this purpose, a simulation experiment set is invented for coating corrosion under insulation in Sinopec Safety Engineering Institute in Qingdao [14], so that simulation experiments can be carried out directly at different heat insulation layers and coatings. Besides, coating corrosions under a circumstance of alternating changes in diverse temperatures and humidity can be simulated. Studies performed by Jiang et al [15]. show that major factors that play an essential role in 20# steel corrosion under insulation include corrosive concentration, and oxygen content and temperature of the environment. Among them, temperature is the most influential factor. Comparing with alternated cooling and heating as well as isoperibol, corrosion degree under a dry-wet alternate environment is more severe.

In contrast to experiment rule researches, the domestic and overseas studies on precaution mainly focus on design, selection and preparation, etc. of thermal insulation materials [16, 17], as well as analysis and detections on those with insulation defects [18, 19], etc. Primarily, the detection on pipelines with a heat insulation layer is performed by means of pulsed eddy current testing [20, 21] which results in a large error and fails to meet practical demands on site. Regarding the study on online monitoring for pipeline corrosion under insulation, rather rough high-risk pipeline location surveys are carried out and it is less likely for online monitoring to be executed. As far as medium/down-stream enterprises in petroleum and petrochemical field are concerned, piping systems with temperature more than 60°C that occupy a proportion of about over 80% in the total number must be coated with insulation constructions. In addition, external and internal corrosions exist under the heat insulation layer simultaneously and the relevant etch state is usually changeable. Obviously, it is rather difficult for corrosion rule studies and offline detections at the earlier stage to meet safety management requirements. Considering this, an online security risk monitoring system is proposed combining RBI technology [22] and integrity management demands in this paper. Regarding the monitoring sensor that serves as an important basis for the system acting as the IoTs, a high-precision quantitative monitoring technology is put forward based on the gamma ray tangential measurement technology.

2 Frame of the Online Corrosion Risk Perception Technology for Process Industry Safety IoTs

Integrity management refers to risk/cost-benefit optimization management on the premise of risk identification during which devices and pipelines of diverse corrosion forms should be classified into several corrosion loops. Then, specific to different corrosion loops, corrosion leakage risk management is conducted. Despite that corrosion loop is a relatively small management object, risks are distributed unevenly in the interior of such a loop. The corresponding risks are mainly gathered in a few of

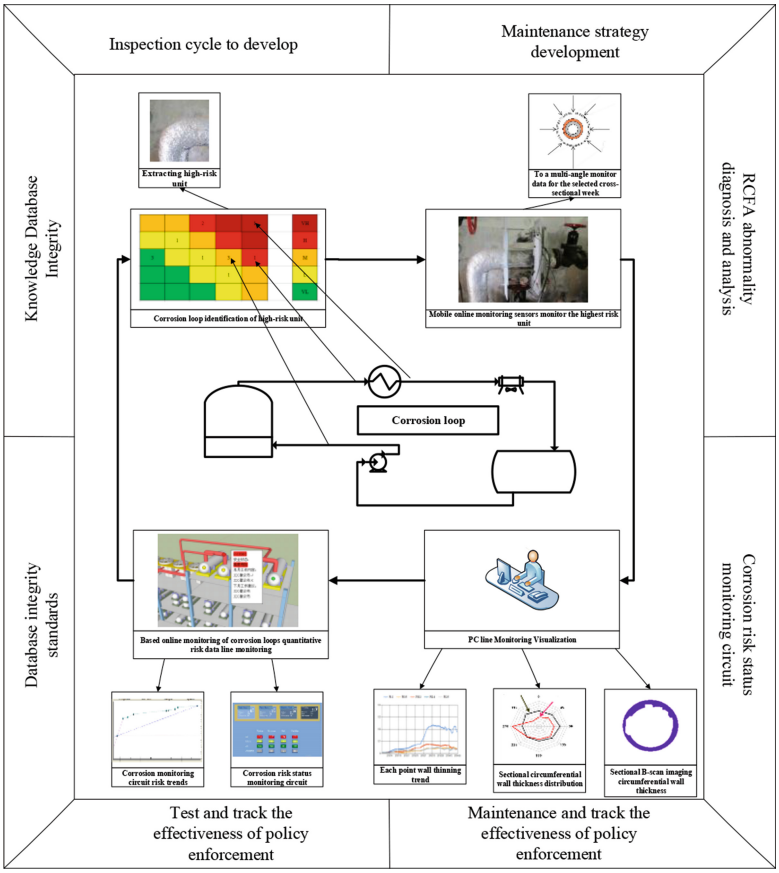

Fig. 1. Frame of online corrosion risk perception system for process industry safety IoTs

devices and pipe units. Therefore, by monitoring the most dangerous units in the loop, the goal of monitoring corrosion leakage risks in the entire loop can be realized. In line with such a principle, a corrosion risk perception system takes shape, as shown in Fig. 1. According to risk identification results of the system, movable wall monitoring sensors are arranged in the most dangerous pipelines located at the corrosion loop, so as to carry out multi-angle measurement for wall thicknesses. Industrial computer in such a monitoring system takes the responsibility to process multi-angle data, analyze circumferential distributions of wall thickness, and ultimately form circumferential B scan image (similar to CT slice photos [23, 24]; in fact, based on the CT technology, tested section slice photos are acquired by adopting ray dose information, Radon transform and Fourier slice theorem [25]). Moreover, locations of measuring points remain unchanged thanks to online monitoring of the sensor. Hence, corrosion trend analysis for various measuring points can be more accurate and reliable. Feedbacks of information obtained through industrial computer analysis are given in the risk analysis module. Through automatic analysis, risk distributions in the corrosion loop are figured

out by this module. As a result, arrangement of the movable wall thickness monitoring sensor can be adjusted regularly, so as to make the corrosion status of the entire corrosion loop become increasingly "transparent". Furthermore, integrity management of such a corrosion loop becomes more reliable and precise.

However, for such a system, one of the most key technologies is such a sensor able to execute movable wall thickness monitoring. It must be applicable to various operating conditions such as high temperature in addition to low disassembly cost and convenient movement. As a result, integrity management cost of an enterprise is prevented from increasing. To sum up, high data reliability, sufficient precision and low cost are fundamental requirements for such monitoring sensors.

3 Principle and Design of Perception Sensor

3.1 Fundamental Principle of Perception Sensor

γ ray is electromagnetic wave with a low wavelength, emitted by decay of radioactive isotopes. Its attenuation during transmission conforms to the Lambert-Beer law [26], as shown in Eq. (1).

$$I = I_0 e^{-\mu_m \rho t} \tag{1}$$

where, I is intensity after the ray penetrates through detection objects; I_0 is intensity before the ray penetrates through detection objects; μ_m is mass-absorption coefficient of absorbing substance vs. γ ray; ρ is density of (absorbing) substance; t is thickness of the substance penetrated through.

According to Eq. (1), the ray with a large enough dose is able to penetrate through substances with a large thickness in theory; residual strength after ray penetration is principally related to both thickness and density of the substance. Theoretically, multiple substances exist simultaneously. As long as certain density differences lie between substances, substances through which the ray penetrates can be determined by technical approaches, such as heat incubation and metallic conduit, etc. Thus, theoretically, γ ray can be adopted to identify interior scaling under insulation of metallic conduits and pipelines, together with figuring out the thickness of both pipes and scale layers, provided that no damages are caused to the heat insulation layer.

In addition, absorption coefficient μ_m of the ray also affects residual strength after ray penetration; moreover, instead of a constant, μ_m is related to compositions of the measured substance, which may exert an enormous influence on wall thickness measurement precision and measured substance measurement. Even, it is likely for it to lead to misjudgment. As a consequence, an appropriate approach should be found to deal with such a problem. According to research findings, when the energy of γ ray exceeds 200 keV, μ_m becomes independent of the compositions of the measured substance. Therefore, under normal circumstances, radiation sources with ray energy ranging from 500 keV to 2500 keV are employed. It can be seemed that, in the case that radiation sources are invariant, the residual strength after ray penetration is only

associated with density and thickness of the measured substance. On this basis, measurement requirements of monitoring sensors can be satisfied.

When the ray energy is large enough, μ_m of each substance is considered to be a constant, so that the residual energy of ray is under the impact of substance density and thickness. Therefore, receipt signals of a monitoring sensor can be calculated in line with the Eq. (2) below.

$$I = I_0 e^{-\sum_{i=1}^{n} \mu_i \rho_i t_i} \tag{2}$$

where, i refers to the categories of substances that the ray goes through. In the case that ray dose I_0 is invariant, density and thickness of the substance penetrated through in the process of ray transmission are variable, accompanied by prompt changes in I, the ray dose received by a ray sensor probe. In theory, when the ray passes a boundary layer, ray dose can be suddenly changed as far as heat insulation layer and metallic conduit ontology are concerned. If such sudden changes can be prominently identified, locations of all boundary layers can be precisely worked out. Obviously, in order to realize high-precision boundary identification, tangential irradiation is an ideal mode for the ray. The relevant reasons can be explained according to Eq. (3) below.

$$T = 2t\sqrt{\frac{D_0}{t} - 1} \tag{3}$$

Where, T is tangential thickness of the measured substance; t is its normal thickness; and, D_0 is the curvature radius of the measured substance boundary layer. In conformity with Eq. (3), it is clear that in the case of $D_0 > 1.25t$, T is larger than t. At this time, tangential ray dose attenuation is also greater than that in a normal direction. In addition, signal mutation of ray dose becomes even more prominent and it is more likely for them to be identified. In other words, boundary layer identification sensitivity and precision of tangential irradiation are higher than that of the normal in theory.

Meanwhile, if a stepping motor is adopted on the normal direction of a boundary layer, the distance (substance thickness or pipeline wall thickness) between two layers can be obtained based on the following Eq. (4).

$$t = pN \tag{4}$$

Where, p refers to the step width of the stepping motor, and N to the number of steps that the stepping motor moves between intervals of two transient signals.

Furthermore, comparing with the method of taking photos, the realization of light sensitive imaging does not rely on a rather high ray hose as far as this approach is concerned. Even a slight dose is able to satisfy identification demands of signal images. Therefore, radiation sources with very low radioactivity can be adopted without affecting the measurement precision. On this basis, security of such a technology is significantly improved, especially in narrow space such as an offshore platform.

3.2 Precision Control and Radiation Dose Selection

In line with the principle of sensor, its precision is under the control of two factors. One is the transmission accuracy of stepping motor; and, the other is the identification precision of photosensitive probe.

Considering the control of a stepping motor on one hand, it is not difficult to realize a precision control of 0.2 mm and below according to the current technical conditions. We can say that as long as stepping step width and transmission ratio are both defined, it is relatively very easy to achieve such a precision.

On the other hand, regarding the counting (measurement of residual radioactive activity) of photosensitive probe, the accuracy of sensor should also be affected. Especially when the activity of radioactive sources is very low, such an impact can be ignored. However, as it is frequently moved and used online for a long term during application, great activity of radioactive sources may incur safety issues. Therefore, a sensor is required to reduce such activity to the greatest extent provided that the corresponding precision has been met.

As required, measurement precision of a sensor is the wall thickness ±0.1 mm. Relying on the Shannin theory, as presented in Eq. (5), the maximum metering error of the whole measurement system should be controlled at ±0.05 mm. As the system measurement precision is influenced by the precision of mechanism motion and positioning as well as the precision of ray measurement, the theoretical measurement precision of the ray must be less than ±0.05 mm with an aim to reach the expected system measurement precision.

$$w_t \leq \frac{w_0}{2} \tag{5}$$

Where, w_0 stands for the expected measurable minimum precision or scale, and w_t for the measurement precision or scale that should be up to at the time of actual measurement.

From a viewpoint of measurement principle, when the system carries out primary measurement by regarding ±0.05 mm as the scale, if the residual radioactive activity changes incurred by it are less than the metering error of this activity, as given in Eq. (6), the system fails to identify that whether such changes are caused by the primary measurement or the counting error of ray measurement. Consequently, measurement precision of such a scale cannot be guaranteed.

$$\Delta I_{0.05} \leq \Delta I_e \tag{6}$$

Where, $\Delta I_{0.05}$ is ray measurement (activity) variation given rise to by a substance thickness of 0.05 mm; and, ΔI_ε is that caused by probe counting error.

On this basis, only when the metering error of residual radioactive activity is less than the residual radioactive activity changes brought about by a measurement based on the minimum measurement scale, the measurement precision of system can be guaranteed. In line with the Shannin theory, the metering error of residual radioactive activity must satisfy Eq. (7) below.

$$\Delta I_e \leq \frac{\Delta I_{0.05}}{2} \tag{7}$$

In the case that the metering error of residual radioactive activity is caused by the counting error, its computing method can be expressed in Eq. (8).

$$\Delta I_e = \frac{N}{\sqrt{n_N}} \tag{8}$$

Where, N is the radioactive activity value of ray, in Bq; and, n_N which is equivalent to $N \times 1$ is its cumulative count value and l refers to the irradiation time in second.

At the time of tangential measurement, the attenuation rule of ray obtained in line with Eq. (1) is expressed in Eq. (9).

$$I = I_0 e^{-\mu T} \tag{9}$$

Where, unit of measurement for I and I_0 is Ci; while μ stands for the attenuation coefficient of measured substance, in mm^{-1}, e for the Napierian base (e = 2.7183).

Dependent on Eqs. (3), (8) and (9), the actual wall thickness metering error given rise to by the radioactive activity metering error of ray is denoted by the following Eq. (10).

$$\Delta t_e = t_r - \frac{D_0 - \sqrt{D_0^2 - \left(\frac{\ln\frac{I \pm \sqrt{\frac{3.7\times10^{10}I}{l}}}{I_0}}{\mu}\right)^2}}{2} \tag{10}$$

Where, t_r is the real value of the actual wall thickness with a unit of mm; Δt_e (unit: mm) is the actual wall thickness deviation caused by radioactive activity metering error.

If Eq. (7) is converted into a criterion for the actual wall thickness, it turns into Eq. (11) shown below.

$$|\Delta t_e| \leq 0.025\,\text{mm} \tag{11}$$

Equations (10) and (11) constitute a radioactive source activity determination criterion of the sensor measurement precision.

4 Performance Test of Monitoring Sensor

The sensor testing machine manufactured according to the operating principle above is illustrated in Fig. 2. This prototype employs a mechanical transmission mechanism.

Fig. 2. Sensor testing machine

4.1 Precision Examination Experiment of Bare Pipe and Coated Pipe

Dependent on standard measurement conditions given in Table 1, Eqs. (10) and (11) are both utilized to make the measurement duration for each point 2 s in line with the relevant application conditions. Then, when the activity of radioactive sources is 20 mCi, the corresponding parameters are presented in Table 1. Concerning the theoretical metering errors of diverse steel pipelines ($\mu = 0.05775$), they are shown in Table 2.

Table 1. Measurement conditions satisfied by design

Piping diameter (mm)	Maximum actual wall thickness (mm)
950	12.7
700	7.94
600	10
500	5.45
450	23.83
400	4.78
350	4.78
300	4.57
250	4.19
200	3.76
150	3.4
100	8.56

Table 2. Error calculation results of actual wall thickness

Piping diameter (mm)	Maximum actual wall thickness (mm)	Positive deviation based actual wall thickness (mm)	Negative deviation based actual wall thickness (mm)	Negative error of actual wall thickness (mm)	Positive error of actual wall thickness (mm)
950	12.7	12.6713	12.7292	−0.0287	0.0292
700	7.94	7.9365	7.94355	−0.0035	0.0035
600	10	9.9950	10.0051	−0.0050	0.0050
500	5.45	5.4490	5.4510	−0.0010	0.0010
450	23.83	23.7922	23.8682	−0.0378	0.0382
400	4.78	4.7794	4.7806	−0.0006	0.0006
350	4.78	4.7794	4.7806	−0.0006	0.0006
300	4.57	4.5695	4.5705	−0.0005	0.0005
250	4.19	4.1896	4.1904	−0.0004	0.0004
200	6	5.9994	6.0006	−0.0006	0.0006
150	5.00	4.9996	5.0005	−0.0004	0.0004
100	8.56	8.5592	8.5608	−0.0008	0.0008

For the experimental motor, the precision error of each step is about 0.01 mm; concerning the gear transmission set, the mean of precision errors ranges from 0.04 mm to 0.05 mm [27]. If computing results obtained in line with Table 2 are taken, the maximum negative and positive errors of actual wall thickness are −0.038 mm and 0.038 mm respectively. In addition, the maximum cumulative measurement error is 0.098, the sum of errors described above. In the case that tests are carried out specific to the most common pipes with a diameter of 150 mm and a measured wall thickness of 5 mm, as given in Fig. 3, the relevant measured value and measured error are 5.12 mm and 0.12 mm accordingly. Based on Table 2, it is clear that the theoretical computing error should be 0.0604 mm calculated according to the precision estimation method put forward in this paper. For such a high estimation precision, it is caused by insufficient error estimation for the transmission of experimental facilities. The maximum positive error is 0.038 mm. Besides, it can be seen from Table 2 that, in most cases, measurement errors of bare pipes are predominant by the mechanical transmission mechanism. Even under a circumstance of low-dose radioactive sources, the counting error of the ray can almost be ignored. However, with the increase in pipe diameter and wall thickness, the counting error also becomes larger. When testing for large caliber pipelines is carried out, such an error has the same order of magnitude as that of mechanical transmission. In this condition, it cannot be neglected.

Regarding the coated pipe under insulation, as shown in Fig. 4, on one hand, the actual thickness and measured thickness of its external insulation layer are 45 mm and 43.86 mm respectively. On the other hand, as far as its metallic conduit is concerned, the corresponding actual wall thickness and measured wall thickness are 6 mm and 6.24 mm. The relevant error is larger than that when it is still a bare pipe, because the coated pipe is subjected to influences of a heat insulation layer and the increase in measured pipe diameter.

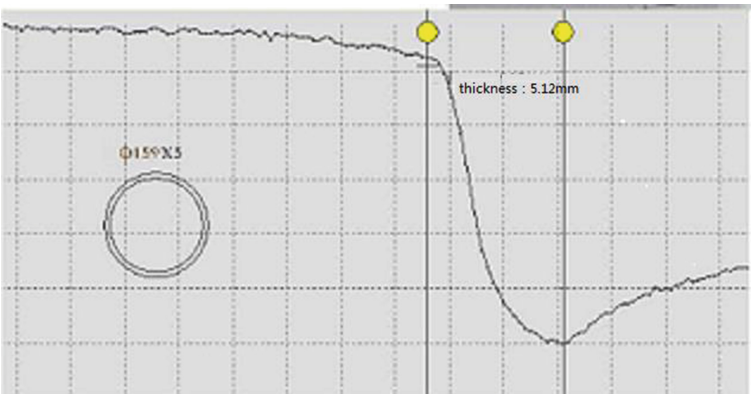

Fig. 3. Measurement result of a bare pipe with diameter 150 mm and wall thickness 5 mm

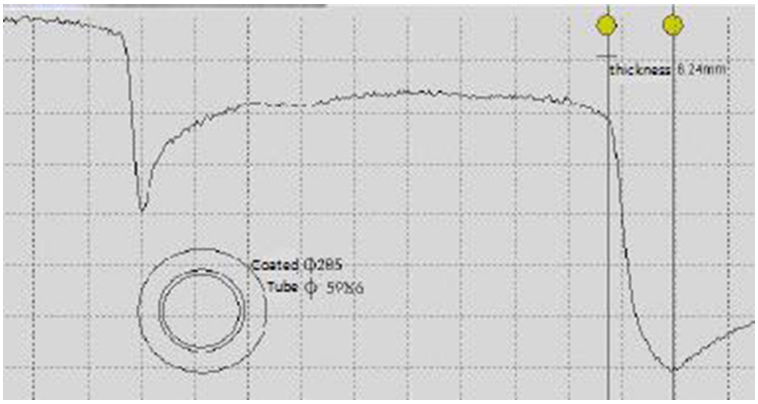

Fig. 4. Measurement result of a coated pipe with diameter 50 mm and wall thickness 6 mm

4.2 Identification and Quantitative Experiments for Boundary Layers in Various Working Conditions

In consistency with the actual monitoring situations, monitored working conditions can be divided to bare pipe, bare pipe + coated pipe, bare pipe + coated pipe + interior scaling, bare pipe + coated pipe + inner media, and bare pipe + coated pipe + interior scaling + inner media. In Figs. 3 and 4, boundary layer identifications for the bare pipe and the bare pipe + the coated pipe have been tested. Below, the testing will be primarily carried out in allusion to the other three conditions which are more complicated.

For the purpose of enhancing testing efficiency, such a monitoring sensor takes advantage of a step-by-step measurement algorithm. In the case that the pipeline is coated with multiple coating layers externally, the entire scanning process is classified into coarse scanning and fine scanning. The former serves as the first step, with an aim

to determine the locations of boundary layers for both the coated pipe and the inner steel pipe; and, the latter is the second step designed to precisely define pipeline wall thickness and the thickness of the interior scaling layer.

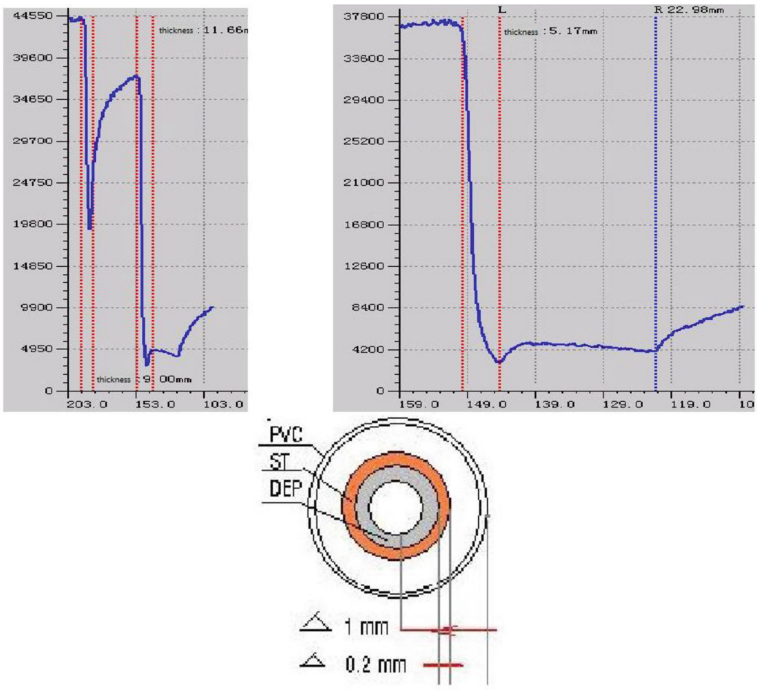

Fig. 5. Measurement result of bare pipe + coated pipe + interior scaling

As for the measurement result of bare pipe + coated pipe + interior scaling, it is given in Fig. 5. During which, CaSO4 colloid is utilized to simulate the actual scaling layer. From Fig. 5, it can be seen that boundaries among PVC, heat insulation layer, metallic conduit and scaling layer can be clearly identified. In detail, that between PVC and heat insulation layer, or, metallic conduit and scaling layer, or, scaling layer and atmosphere, has a V-shaped inflection point; in comparison, a reverse V-shaped inflection point occurs to the boundary layer of heat insulation layer and metallic conduit. In terms of the thickness measurement, measured thickness of the pipe is 5.17 mm. In fact, the actual wall thickness of the pipe is 5 mm. In addition, the measured thickness of the interior scaling substances is 17.81 mm, instead of 20 mm which is their practical thickness. By contrast to the bare pipe, error of the metallic conduit goes up, while the measurement error of scaling layer lies within an acceptable range.

In addition to conveying gas, some pipes also play a role of transporting liquids. Apparently, the density of the latter is higher than the former. In line with Eq. (1), its ray absorption rate is also significantly higher than gases. Therefore, under a

circumstance that a pipeline contains liquids inside, V-shaped inflection point between metal and liquid should be tested to determine whether it is as ideal as what has been shown in Fig. 5. During experiment, water whose density is greater than common substances in general pipelines is adopted to test its impacts in extreme cases. The corresponding test results are demonstrated in Fig. 6.

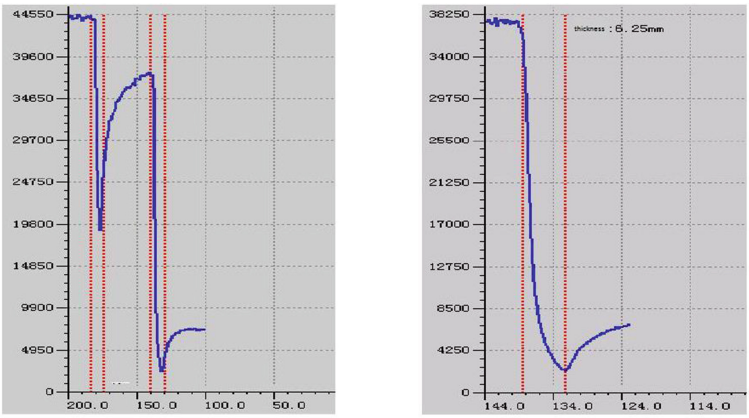

Fig. 6. Measurement result of bare pipe + coated pipe + water as interior medium

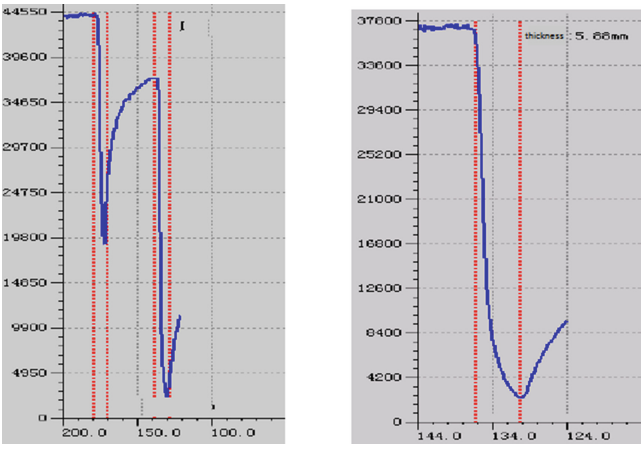

Fig. 7. Measurement result of bare pipe + coated pipe

Based on Fig. 6, due to the existence of a considerable gap between densities of metallic conduit and water, V-shaped curve for its boundary layer becomes even more obvious. However, if compared with the inflection point for metal and gas shown in Fig. 7, it appears much less weak, indicating that when densities for substances on both sides of the boundary layer are close to each other, more effective sharpening algorithm

is required to identify the inflection point of signal curves. In addition, relative to results presented in Fig. 4, measurement thickness of the pipe is 6.25 mm provided that liquid medium exists inside it, as shown in Fig. 6. The corresponding wall thickness measurement error that has a little impact can nearly be ignored if compared with the testing results obtained in a gaseous environment.

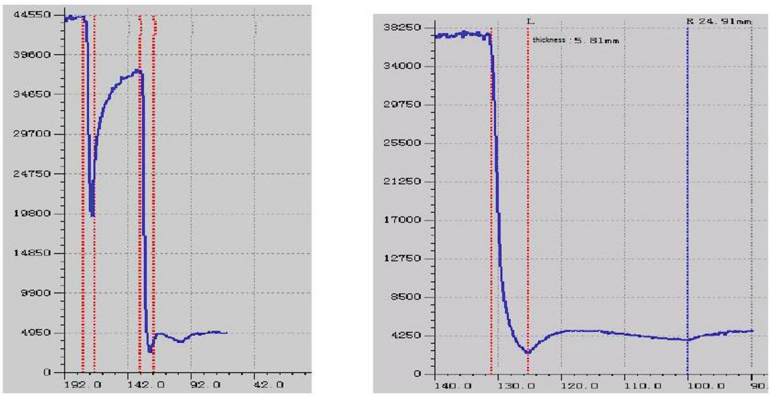

Fig. 8. Measurement result of bare pipe + coated pipe + scaling + water as interior medium

From Fig. 8, owing to the existence of liquid, it becomes more difficult to determine the boundary layer between scaling layer and interior media; moreover, the V-shaped inflection point also seems to be gentle. What needs to be noted is that they can be still identified in processes of coarse and fine scanning.

5 Conclusions

(1) The online corrosion monitoring technology designed in this paper is applicable to all monitored working conditions currently encountered. At the time of measuring boundary layers among substances, V-shaped curves can be utilized to perform accurate identification. As under a significant influence of densities for substances on each side of the detected boundary layer, the closer such densities are to each other, the gentler such V-shaped curves will be. In this case, better sharpening algorithms are needed to identify them.

(2) This monitoring technology has a rather high thickness measurement precision 0.1 mm higher than ultrasonic thickness measurement. At a later period, if a more precise electrical transmission system is employed, the corresponding precision will be substantially improved, so that diverse demands during process industry integrity management can be satisfied.

References

1. Smith, T.F., Waterman, M.S.: Identification of common molecular subsequences. J. Mol. Biol. **147**, 195–197 (1981)
2. May, P., Ehrlich, H.-C., Steinke, T.: ZIB structure prediction pipeline: composing a complex biological workflow through web services. In: Nagel, W.E., Walter, W.V., Lehner, W. (eds.) Euro-Par 2006. LNCS, vol. 4128, pp. 1148–1158. Springer, Heidelberg (2006). https://doi.org/10.1007/11823285_121
3. Foster, I., Kesselman, C.: The Grid: Blueprint for a New Computing Infrastructure. Morgan Kaufmann, San Francisco (1999)
4. Czajkowski, K., Fitzgerald, S., Foster, I., Kesselman, C.: Grid information services for distributed resource sharing. In: 10th IEEE International Symposium on High Performance Distributed Computing, pp. 181–184. IEEE Press, New York (2001)
5. Foster, I., Kesselman, C., Nick, J., Tuecke, S.: The physiology of the grid: an open grid services architecture for distributed systems integration. Technical report, Global Grid Forum (2002)
6. National Center for Biotechnology Information. http://www.ncbi.nlm.nih.gov
7. Fitzgerald, B.J., Stefan, W.: A corrosion under insulation prevention strategy for petrochemical industry piping. J. Corros. Manag. **57**, 15–19 (2004)
8. Li, J.: Under insulation corrosion protection and aluminum cold spray technology. J. Shanghai Paint. **46**, 19–22 (2008)
9. Susan, C., Faisal, K., John, S.: Analysis of pitting corrosion on steel under insulation in marine environments. J. Loss Prev. Process Ind. **26**, 1466–1483 (2013)
10. Bruce, R.: Preventing corrosion under insulation in chemical manufacturing facilities. J. JPCL **5**, 40 (1998)
11. Lv, X.-L., Tang, J.-Q., Gong, J.-M., et al.: Under insulation corrosion protection. J. Corros. Sci. Prot. Technol. **26**, 167–172 (2014)
12. Geary, W.: Analysis of a corrosion under insulation failure in a carbon steel refinery hydrocarbon line. J. Case Stud. Eng. Fail. Anal. **1**, 249–256 (2013)
13. Kane, R.D., Ashbaugh, W.G., Mcgowan, N., et al.: New industry standards, test procedures, and surface treatments combat corrosion under insulation. In: Corrosion Source-2000 Online Symposium, Washington, p. 403 (2000)
14. Norsworthy, R., Dunn, P.J.: Corrosion under thermal insulation. J. Mater. Perform. **41**, 38 (2002)
15. Qiu, Z.-G., Liu, X.-H., Qi, J., et al.: Under insulation corrosion coating simulation equipment. Technical report, Corrosion Forum (2015)
16. Jiang, Y.-J., Gong, J.-M.: Under insulation corrosion behavior of 20 steel under different simulated conditions. J. Mater. Mech. Eng. **35**, 66–70 (2011)
17. Li, J., Lin, R.-F., Chang, Y.-P.: Material selection and design of foam insulation jacket corrosion. J. Corros. Prot. **29**, 80–83 (2008)
18. Folke, B., Tomas, E.: Properties of thermal insulation materials during extreme environment changes. J Constr. Build. Mater. **23**, 2189–2195 (2009)
19. Xin, W., Ding, K.-Q., Huang, D.-L., et al.: Pulsed eddy current testing technology simulation with the insulation pipeline corrosion defects. J. Nondestruct. Test. **31**, 509–512 (2009)
20. Ren, Z.: The new technology to detect corrosion under insulation pipeline. J. Foreign Oil Field Eng. **18**, 53–54 (2002)
21. Wu, X., Li, F.-Q., Shi, K., et al.: Pulsed eddy current thickness measurement technology. J. Nondestruct. Test. **7**, 528–530 (2009)

22. Zhao, L., Chen, D.-F., Lu, Y., et al.: Application of pulsed eddy current in the metal thickness detection. J. Meas. Control Technol. **12**, 22–24 (2007)
23. Stephane, B., Anne, K.: Dynamic X-ray computed tomography. J. Proc. IEEE **91**, 1574–1588 (2003)
24. Zhao, J.-H., Qu, Z.: Industrial CT tomographic image sequence to achieve a two-dimensional re-Zhong. J. Computer development **13**, 20–22 (2003)
25. Zhang, S.-L.: Algebraic Reconstruction Method Research and Application of industrial CT image. Northwestern Polytechnical University, Xi'an (2004)
26. Wei, W.-S.: Ray fault diagnosis. J. Petrochem. **32**, 700–702 (2003)
27. Munro, R.G., Palmer, D.: Gear transmission error outside the normal path of contact due to corner and top contact. J. Mech. Eng. Sci. **213**, 389–400 (1999)